Methanol Dehydrogenation on Pt Electrodes: Active Sites and Role of Adsorbed Spectators Revealed through Time-Resolved ATR-SEIRAS

Laura Pérez-Martínez, Laura M. Machado de los Toyos,† Jani J. T. Shibuya, and Angel Cuesta.*

School of Natural and Computing Sciences, University of Aberdeen, Aberdeen AB24 3UE, Scotland, UK

KEYWORDS

Methanol; adsorbed CO; spectators; ATR-SEIRAS; spectrokinetics

ABSTRACT

The dynamics of methanol dehydrogenation to adsorbed CO (CO_{ad}) on polycrystalline Pt in the hydrogen underpotential adsorption (H_{upd}) region has been investigated under potentiostatic conditions using time-resolved ATR-SEIRAS after a potential step. Our experiments reveal that the electrooxidation of methanol to CO_{ad} is possible at potentials at least as negative as 0.01 V vs. RHE and occurs nearly exclusively at (111)- and (100)-oriented defect sites, whereby (111)-oriented defects show higher activity unless blocked by spectator species. Under conditions in which, due to a combination of low methanol concentration and sufficiently negative potential, the

formation of CO_{ad} is very slow, we have been able to determine the singleton frequency of linearly bonded CO_{ad} (CO_L) on Pt (2002 cm^{-1} ± 2 between 0.01 and 0.06 V). Under these conditions, the slow increase in the coverage of CO_{ad} (θ_{CO}), as revealed by the increase of the integrated intensity of the bands corresponding to CO_L and bridge or multiply bonded CO_{ad} (CO_B/CO_M), is not accompanied by an increase in the CO_L stretching frequency (ν_{CO_L}), which initially remains constant and then increases sharply, an effect that repeats itself several times, giving rise to a staircase-like increase of ν_{CO_L} before it starts to increase monotonously in parallel with θ_{CO}. We attribute this behaviour to the progressive population of terraces by CO_{ad} diffusing from the defect sites where it has been formed. We also detected under these conditions a band at 1677 cm^{-1} which we attribute to adsorbed formyl (HCO_{ad}) and which we suggest is the last intermediate in the oxidation leading from methanol to CO_{ad}. Our experiments also allow the direct spectroscopic determination of the rate of formation of CO_{ad} at the limit of zero coverage ($\theta_{CO} \rightarrow 0$), from which Tafel plots revealing the potential dependence of the reaction rate when $\theta_{CO} \rightarrow 0$ can be drawn. These plots, together with the potential dependence of the time elapsed between the first observation in spectra of CO_B/CO_M and that of CO_L, provide evidence of the important role played by adsorbed spectators in determining the reaction rate.

1. INTRODUCTION

Methanol can be obtained from renewable sources and can be easily handled, stored, and transported. Moreover, it can be used as fuel in direct methanol fuel cells (DMFCs), which explains the extensive and intensive research on methanol oxidation over the past five decades.[1–9] Pt or Pt-based materials are the best catalysts known for this reaction[10,11] but, unfortunately, a stable partially oxidised product which strongly adsorbs on Pt (and other metals), namely

adsorbed carbon monoxide (CO_{ad}), is formed in one of the two parallel paths along which the reaction can proceed,[1,4,12,13] poisoning the catalyst.

In trying to solve this problem, the most common strategy has been to explore catalytic materials on which CO_{ad} can be oxidised at less positive potentials or on which CO adsorption is weaker.[14–16] Alternatively, CO poisoning can be avoided if the reaction mechanism and the role of specific surface sites are known in sufficient detail as to engineer the catalyst surface at the atomic level with the goal of inhibiting the formation of CO_{ad} while maintaining a high activity towards the total oxidation of methanol to CO_2 through the direct path. Intense experimental and computational efforts have been devoted to trying to understand the finest details of the electrocatalytic dehydrogenation of methanol on platinum, including the effect of the surface structure on the thermodynamics and kinetics of the reaction[17–22] and efforts aimed at unveiling the mechanism of the electrocatalytic oxidation of methanol to adsorbed CO.[23–26] Using Pt(335), a stepped single-crystal electrode composed of 4-atom wide (111) terraces separated by (100)-oriented monoatomic steps, Shin and Korzenieski[17] were able to prove, using external infrared reflection-absorption spectroscopy (IRAS), that (111) terraces are essentially inactive for methanol dehydrogenation in the hydrogen underpotential adsorption (H_{upd}) region, while CO_{ad} resulting from partial oxidation of methanol appears on (100) step sites at potentials as negative as 0.06 V *vs.* RHE, deep into the H_{upd} region and just before the onset of hydrogen evolution. However, due to the constraints associated with the thin-layer configuration required for IRAS, that early work provides a static picture, a snapshot of the process which cannot describe the dynamics of the occupation of the different adsorption sites present on the surface. The higher activity of step sites for methanol dehydrogenation was confirmed later by Housmans and Koper[18,27] based on chronoamperometric experiments, using in this case single-crystal electrodes

containing (111) terraces and (111)-oriented steps (which can also be considered as (110)-oriented; please note that in both cases this is a purely geometric description of the step). Chronoamperometric measurements by Grozovski et al.[19] using single-crystal electrodes composed of (111) terraces separated by either (100)- or (111)-oriented monoatomic steps as well as (100) terraces separated by (111)-oriented steps revealed that (100) terraces are more active than (111) domains, and confirmed that step sites, whether (100)- or (111)-oriented are the most active sites. However, at least in the potential region studied by them, > 0.3 V *vs.* RHE, the difference in activity for CO_{ad} formation between (100) domains and (111) steps in Pt(S)[*n*(100) x (111)] was shown to be small and, actually, for sufficiently narrow terraces Pt(100) was poisoned faster than the corresponding stepped surfaces, which led Grozovski et al. to suggest that (100) sites/domains are in general more active for methanol dehydrogenation than (111) ones. Another relevant piece of information was provided by our own group[23,24] proving that a minimum atomic ensemble of three contiguous Pt atoms is required for the dehydrogenation of methanol to CO_{ad}.

Another important aspect to which less attention has been paid is that of the role played by spectator species, like specifically adsorbing anions, in the electrocatalytic dehydrogenation of methanol. Spectator species, although not involved in the reaction mechanism, can block reaction sites. We can therefore expect different behaviour when working in the presence or absence of a specifically adsorbing anion, like, *e.g.*, sulphate, in the electrolyte. Even in the absence of specifically adsorbing anions, as in, *e.g.*, perchloric acid solutions, spectator species like adsorbed OH (OH_{ad}) can be formed from water. Different spectator species adsorb with different strength on Pt surfaces. For example, in acidic solutions, sulphate starts adsorbing on Pt(111) surfaces around 0.35 V *vs.* RHE (please note that this will depend on the sulphate

concentration) while OH_{ad} is absent below 0.6 V *vs.* RHE. Even more important, the same spectator will adsorb more strongly on some kind of sites than on others. For example, while both sulphate and OH adsorption can only start on Pt(111) surfaces once H_{upd} has been completely desorbed, OH and sulphate adsorption overlap hydrogen desorption in (100)-terrace, (100)-steps and (111)-step sites.[28,29] Because, as discussed above, (111) and (100) defects and terraces are the active sites for methanol dehydrogenation, the adsorption of spectator species on these sites can be expected to have an effect on the reaction rate.

Despite these advances, the atomistic details of the electrocatalytic dehydrogenation of methanol are still largely unknown. Deeper knowledge about active sites, the progressive population of different sites on the electrode surface and how adsorption of spectator species in each kind of sites affects the progression of the reaction is needed, and this requires dynamic spectroscopic studies which, with some rare exceptions,[25] are largely missing.

Here we present the results of a study in which chronoamperometric transients following a potential step were monitored using time-resolved surface-enhanced infrared absorption spectroscopy in the attenuated total reflection mode (ATR-SEIRAS). The high sensitivity of this technique allows detection in real-time of changes in the CO coverage[30,31] and the determination of some kinetic parameters.[32–34] Experiments were limited to the potential region in which dehydrogenation of methanol to CO_{ad} is the only reaction occurring, without interference of either the direct path or further oxidation of CO_{ad} to CO_2. The high time resolution achieved allows to monitor the progressive population of different sites on the electrode surface, and comparison between experiments performed in $HClO_4$ and H_2SO_4 reveals important information related to the role of spectator species.

2. EXPERIMENTAL SECTION

Electrolytes were prepared by dissolving H_2SO_4 (96%, Merck Suprapur) or $HClO_4$ (70%, Merck p.a EMSURE) in ultrapure water (Milli-Q) up to a concentration of 0.1 M (approximate pH 1). Solutions containing methanol were prepared by adding methanol (Honeywell CHROMASOLV) to the desired concentration. All the experiments were performed using N_2 purging at room temperature. A flame-annealed Pt wire (Alfa Aesar, 99.997% metals basis) was used as counter electrode and a home-made Ag/AgCl (KCl_{sat}) electrode as reference. However, all the potentials in the text are referred to the reversible hydrogen electrode (RHE), unless otherwise stated. The working electrode for the cyclic voltammogram in Figure 1(A) was a polycrystalline platinum rod (Metrohm, 0.3 cm in diameter) embedded in teflon and attached to a Metrohm 628-10 rotating electrode. The rod's exposed circular face was polished with MasterPolish (Buehler, Alumina + SiO_2, 0.05 μm) and then sonicated in Ultrapure water before each experiment. Typical CVs of polycristalline Pt films on Si in both 0. 1 M $HClO_4$ and 0.1 M H_2SO_4 are provided in the in the Supporting Information, Fig.S1.

ATR-SEIRA spectra were recorded using a Nicolet iS50R FTIR spectrometer equipped with a liquid nitrogen-cooled MCT detector and a home-made ATR accessory, using unpolarized light. A new reference spectrum was recorded before each spectral series at 0.91 V vs RHE when H_2SO_4 was the electrolyte and at 0.96 V when $HClO_4$ was used as electrolyte. The potential of the background spectrum was chosen positive enough to have any present CO_{ad} oxidised before starting the experiment [35–37] while minimising changes in the baseline of the spectra. Differential spectra are reported in absorbance units (a.u.), calculated as -log $\left(\frac{R_{\text{sample}}}{R_{\text{reference}}}\text{-}\right)$, where $R_{\text{reference}}$ and R_{sample} are the reference and sample spectra, respectively. Positive bands correspond to species

present in the sample spectrum that were absent in the reference spectrum, while negative bands correspond to species present in the reference spectrum that are absent in the sample spectrum. Series of differential spectra after a potential-step were obtained in the kinetics mode by accumulating 1 or 2 interferograms per spectrum with a spectral resolution in the range between 4 and 32 cm^{-1}. An adequate combination of these two parameters allowed to achieve a sufficiently high time resolution with a good signal-to-noise ratio for each specific experiment. The specific parameters used in each of the experiments presented in this work are provided in the corresponding figure captions. The working electrode was a Pt film deposited on the totally reflecting plane of a Si prism beveled at 60° following a previously reported procedure. [38] The Si prism was attached to the spectroelectrochemical cell using an O-ring seal and electrical contact with the film was made by pressing onto it a circular platinum wire. Before any IR measurements, the film was cycled in the corresponding electrolyte to check its stability, then rinsed with Milli-Q water before filling the cell with the solution containing the target concentration of methanol.

3. RESULTS AND DISCUSSION

Fig. 1A shows the CVs of polycrystalline Pt in both 0.1 M H_2SO_4 (black line) and 0.1 M $HClO_4$ (red line) within the potential range between 0.01 and 0.46 V, which encompasses the H_{upd} region plus the negative end of the double-layer region. Characteristic chronoamperometric transients recorded simultaneously with the time-resolved ATR-SEIRA spectra in the presence of 0.01 M CH_3OH after a potential step from 0.91 V (0.1 M H_2SO_4) or 0.96 V (0.1 M $HClO_4$) are presented in Fig. 1B for 0.1 M H_2SO_4 solutions and in Fig. 1C for 0.1 M $HClO_4$.

The oxidation of methanol to CO_{ad},

$$CH_3OH \longrightarrow CO_{ad} + 4H^+ + 4e^- \quad (1)$$

must result in a positive current and, at sufficiently positive potentials a positive current is recorded indeed, often at relatively long times which become shorter with increasingly positive potential (please note that traces of oxygen in the electrolyte result in a negative current contributing to the transient even at very long times, particularly in the experiments in 0.1 M $HClO_4$). Even when such a positive current transient is observed, the current slowly decays to zero, which is to be expected because reaction (1) is a self-poisoning process in which the product blocks the surface for further reaction events. It is therefore the reaction rate at time zero, before the product of the reaction has started blocking the surface, that we are interested in. However, at very negative potentials, at which reaction (1) can be expected to be very slow, measuring the resulting very small current can be very challenging. Even at potentials at which reaction (1) results in a large enough positive current, the transient contains, in addition to the double-layer charging current, other contributions which make extraction of kinetic information corresponding to the rate of reaction (1) at time zero a difficult, if not impossible, task. At very short times, reduction of the thin oxide film formed at the potential from where the step is made:

$$PtO_x + 2xH^+ + 2xe^- \longrightarrow Pt + xH_2O \quad (2)$$

and, at potentials < 0.35 V, adsorption of H_{upd}:

$$H^+ + e^- \longrightarrow H_{upd} \quad (3)$$

will contribute a negative current to the transient. Also, at these potentials and at slightly longer times, in addition to reaction (1), the displacement of H_{upd} formed in reaction (3) by CO_{ad} generated from methanol dehydrogenation will result in an additional positive contribution to the current transient:

$$CH_3OH + xH_{upd} \longrightarrow CO_{ad} + (4 + x)H^+ + (4 + x)e^- \quad (4)$$

On the contrary, infrared spectroscopy allows to focus on the growth of the vibrational bands of CO_{ad} and to extract the reaction rate from the rate with which they grow without any interference of other simultaneous processes.

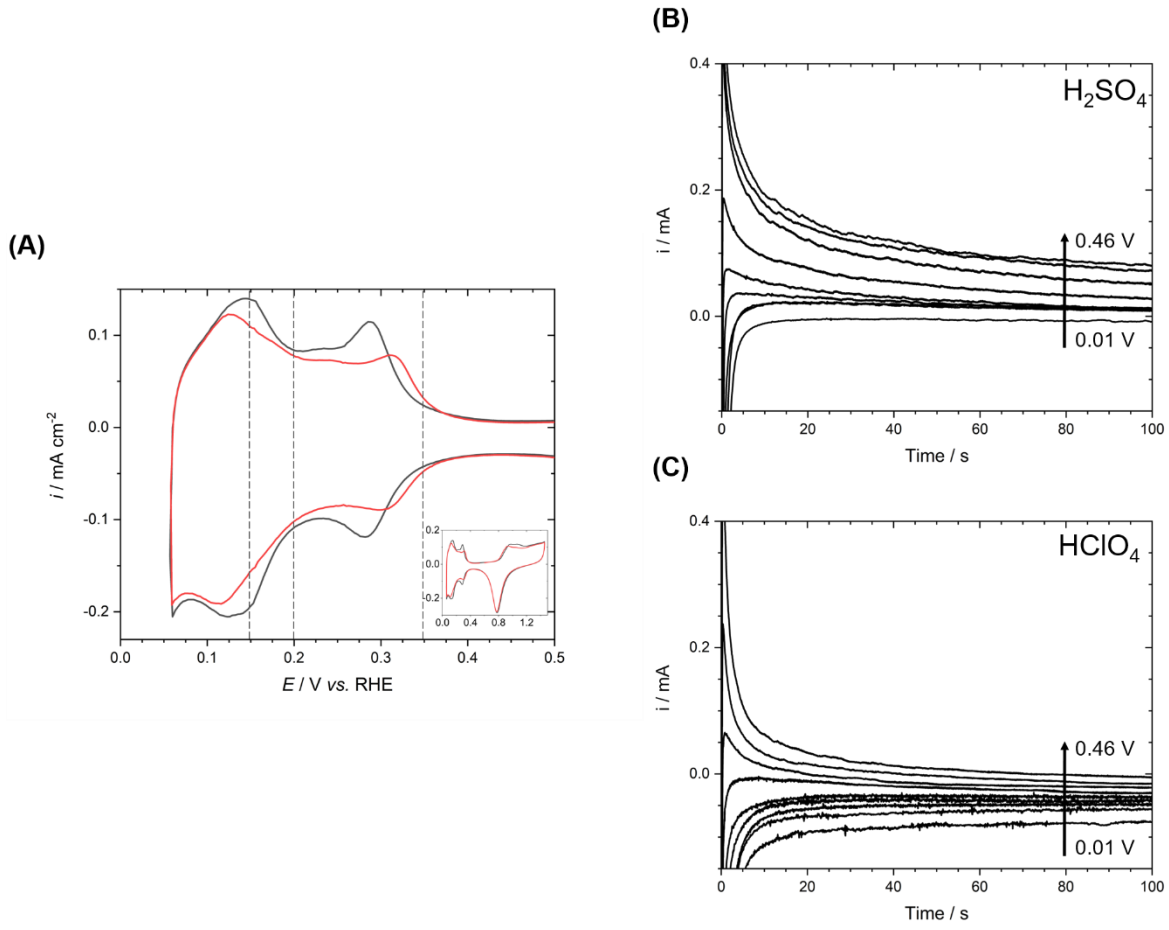

Figure 1. **(A)** Zoom into the region between 0.05 and 0.5 V of the CV of a polycrystalline Pt electrode in 0.1 M H_2SO_4 (black line) and 0.1M $HClO_4$ (red line) at 0.05 V s^{-1}, corresponding to the potential region where the formation of CO_{ad} was monitored using time-resolved ATR-SEIRAS. The whole CV is shown in the inset. The dashed grey vertical lines mark specific potentials which are important in further discussion. Characteristic current transients recorded simultaneously with the ATR-SEIRA spectral series in 0.1 M CH_3OH solutions in 0.1 M H_2SO_4

(B) and 0.1 M $HClO_4$ **(C)** after a potential step from either 0.91 V **(B)** or 0.96 V **(C)** to a potential between 0.01 and 0.46 V.

Any electrochemical cell needs some time, given by the product of the interfacial capacitance times the uncompensated electrolyte resistance (*i.e.*, by the cell's time constant), to establish the new interfacial potential profile after a potential step from a different potential, due to the necessity to charge the electrical double layer. In our system, the time required to reduce the platinum oxide formed at the initial potential (Equation 2) and, if the final potential falls within the H_{upd} region, the time needed to adsorb hydrogen up to the corresponding equilibrium coverage, will also contribute to delay the establishment of the new, final, potential profile (effectively, the platinum oxide reduction and hydrogen adsorption processes behave as an additional capacitance in parallel with that corresponding to the double layer that increases the cell's time constant). We need therefore to be sure that the process monitored by ATR-SEIRAS following the building up of CO_{ad} on the electrode surface starts once the double-layer charging has been completed and the interfacial potential profile corresponding to the sample potential has been properly established. Fig. S2 in the Supporting Information shows transients in methanol-free 0.1 M H_2SO_4 after a potential step from 0.91 V to the sample potentials used in our ATR-SEIRAS experiments (nearly identical transients were obtained in 0.1 M $HClO_4$). Table S1 in the Supporting Information reports the time at which a CO_{ad} band was observed for the first time in the corresponding spectral series after a potential step in methanol-containing solutions. Comparison of Fig. S1 with the data in Table S1 confirms that recording of the time evolution of the CO_{ad} bands in the spectral series started once the interfacial potential profile had been properly established.

Fig. 2A shows a typical time-resolved ATR-SEIRA spectral series recorded after a potential step from 0.91 V to 0.16 V in 0.1 M H_2SO_4 containing 0.01 M CH_3OH with a time interval of 190 ms. For the sake of clarity, only the first approximately 30 s and the interval from 75 s to 85 s are shown. Because in some of the spectral series, there is a considerable time between the beginning of the series (which coincides with the potential step) and the first observation of a CO_{ad} band, time cero has been set as that corresponding to the last spectrum in the series just before the first observation of a CO_{ad} band. Otherwise, analysis of the rate of formation of CO_{ad}, which is based on the time derivative of the integrated intensity *vs.* time curves of the CO_{ad} bands, would have included a period of time with an apparent but not real zero rate of CO_{ad} formation (if the rate of formation were indeed zero CO_{ad} would never build up) in which θ_{CO} is simply below the detection limit. That this does not introduce any artefact in our analysis of the data presented in Figs. 2 to 7 is confirmed by the observation that, at sufficiently low coverage, the rate at which CO_{ad} builds up remains constant over a relatively wide range of θ_{CO} (see Fig. 4). This observation implies that the coverage within that regime is large enough to be over our detection limit but low enough as to not have a surface blocking effect for the oxidation of methanol to CO_{ad}. We can therefore be 100% certain that the rate of formation of CO_{ad} at even lower coverages below our detection limit will be the same as in that region and correspond to the limit at $\theta_{CO} = 0$. It is therefore correct to extrapolate the derivative of the integrated absorbance transient to the time corresponding to the first spectrum before observation of a CO_{ad} band to obtain the rate of formation of CO_{ad} when $\theta_{CO} = 0$. Further evidence supporting the correctness of our approach is provided by the excellent agreement between the potential dependence of the rate of formation of CO_{ad} reported by us above 0.3 V and that reported in (25),

where the experiments did not involve a potential step. (Please note that no experiment below 0.3 V was reported in (25) and that experiments there were only performed in 0.1 M $HClO_4$.)

Three spectral features, highlighted in Figs. 2C, D and E with selected spectra at specific times as specified in the figure, are easily identifiable and are observed in all spectral series. The band with frequency which blue-shifts from 2005 to 2059 cm^{-1} as the intensity increases with time (Fig. 2D) corresponds to the C-O stretching of linearly adsorbed CO on Pt (CO_L), while the broad band appearing initially at 1787 cm^{-1} and splitting later into two contributions at 1787 and 1885 cm^{-1} (Fig, 2E) corresponds to the C-O stretching of bridge- (CO_B, component at the higher frequency) and multiply-bonded (CO_M, band at 1787 cm^{-1}) CO_{ad}. Following Yan et al.,[39] CO_M and CO_B will be considered jointly (CO_B/CO_M) when integrating the band intensity for analysis of the rate of formation of CO_{ad}. Finally, the band at 3656 cm^{-1} which appears at intermediate to high CO coverage (θ_{CO}) corresponds to the O-H stretching mode of interfacial water on Pt covered by a dense adlayer of CO_{ad} (Fig 2C).[40–43] The evolution of the integrated intensity of the CO_L band (I_{CO_L}, black) and of the CO_B/CO_M band (I_{CO_B/CO_M}, red) with time during the complete series is shown in Fig.2B. In the following sections, we will analyse in detail the evolution of these bands with time and how the potential, methanol concentration and the adsorption of either OH or sulphate affect the process of methanol dehydrogenation to CO_{ad}.

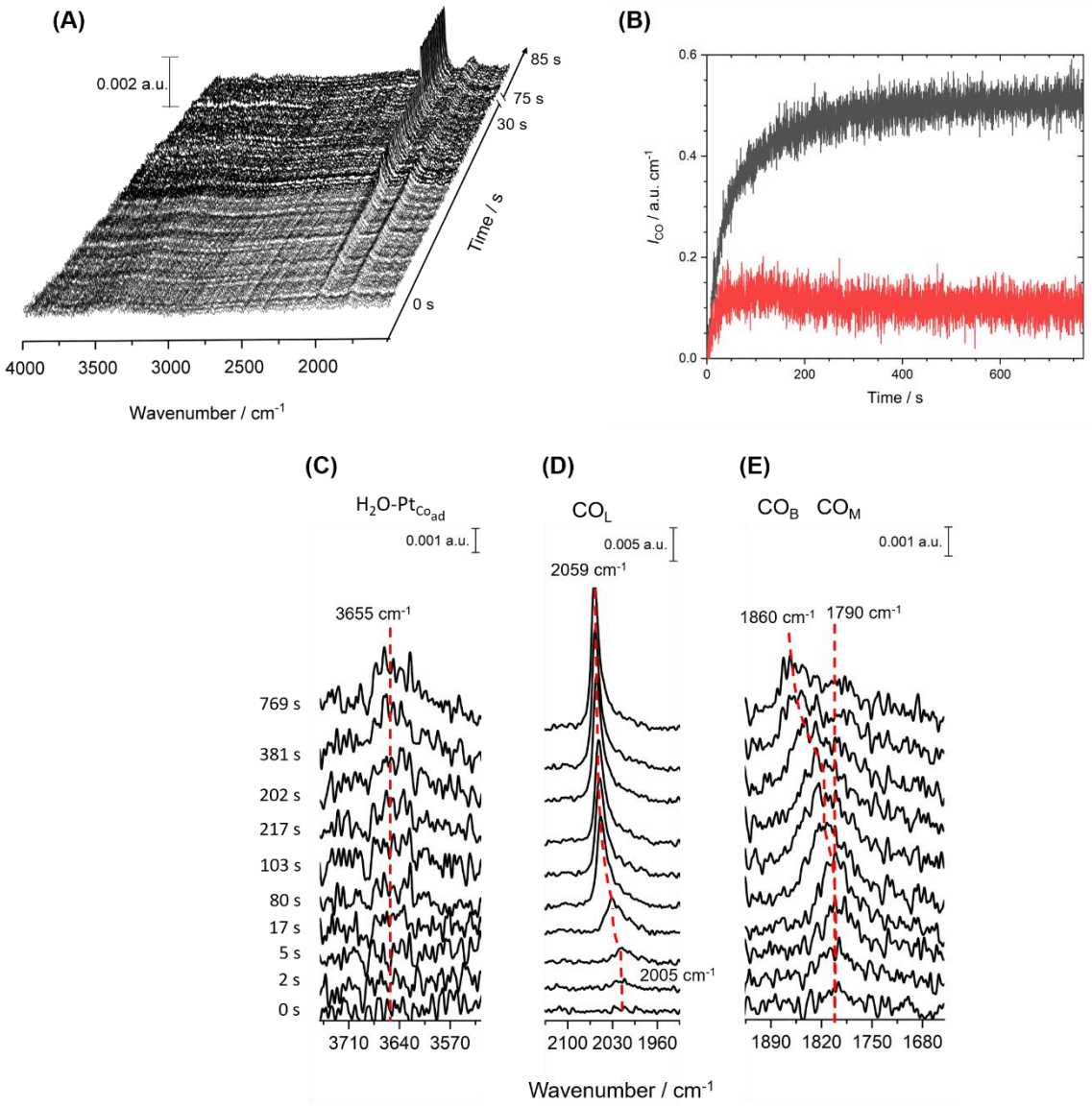

Figure 2. **(A)** Typical time-resolved ATR-SEIRA spectral series of Pt-in 0.1 M H_2SO_4 containing 0.01 M CH_3OH recorded after a potential step from 0.91 V vs. RHE to 0.16 V vs. RHE. Each spectrum consists of a single interferogram recorded with a spectral resolution of 4 cm^{-1}, resulting in a time interval between spectra of 0.19 s. Only the first approximately 30 s and the interval from 75 s to 85 s are shown. The reference spectrum was taken at 0.91 V. **(B)** Time dependence of I_{CO_L} (black) and $I_{CO_{B/M}}$ (red). **(C)**, **(D)** and **(E)** selected spectra extracted from the

series at times as specified in the figure in the spectral region corresponding to the O-H stretching of water **(C)**, the C-O stretching of CO_L **(D)** and the C-O stretching of CO_B/CO_M **(E)**.

3.1. Formation of CO_L and CO_B/CO_M and detection of an intermediate species. Our Pt film is polycrystalline and can therefore be expected to contain a large multiplicity of sites, dominated by defect sites of (111) and (100) orientation (hydrogen ad/desorption peaks just below 0.15 and 0.30 V, respectively, in the CV in Fig. 1) and possibly some small (111) domains (the more or less constant-current contribution in the H_{upd} region of the CV in Fig. 1). In addition, CO can adsorb either as CO_L or as CO_B/CO_M, and it is, therefore, worth exploring if CO_{ad} generated from methanol dehydrogenation shows any preference at all for any of these two geometries.

The top panels of Figs. 3A and B show how the delay between the first spectrum in which CO_B/CO_M is observed and the first observation of a CO_L band depends on the applied potential in 0.1 M $HClO_4$ and 0.1 M H_2SO_4, respectively. Selected spectra in the presence of 0.01 M methanol are shown in the lower panels of Fig. 3. Interestingly, while at potentials below 0.1 – 0.16 V, both in sulphuric and perchloric acid CO_L and CO_B/CO_M appear simultaneously within our time resolution (although the ratio between the intensity of the CO_L and CO_B/CO_M bands is much smaller than at high coverage, a well-known fact[39,44–46]), once this potential is reached, CO_B/CO_M is clearly preferred over CO_L which, when a concentration of methanol 0.01 M in perchloric acid is used, takes as much as 30 s longer to appear on the electrode surface than CO_B/CO_M. A recent time-resolved ATR-SEIRAS study of the adsorption of CO on Pt electrodes in the same potential range on which this study has focused found that CO_L sites are occupied first, CO_B/CO_M appearing slightly later.[47] Therefore, the behavior observed here has to be connected with the activity and availability of specific sites for the dehydrogenation reaction and how that availability is determined by the applied potential.

In both perchloric and sulphuric acid solutions, the delay between the formation of CO_B/CO_M and that of CO_L decreases with increasing methanol concentration. In 0.1 M $HClO_4$, the potential interval in which formation of CO_B/CO_M is preferred over CO_L is relatively narrow, and at 0.41 V (0.36 V if $C_{methanol} > 0.04$ M) again no preference for CO_L or CO_B/CO_M can be observed within our achievable time resolution. On the contrary, in 0.1 M H_2SO_4, the maximum delay between the first observation of CO_B/CO_M and that of CO_L is smaller at all methanol concentrations, the maximum delay tends to be observed at slightly more positive potentials and a slight preference for CO_B/CO_M is observed even at the most positive potential (0.46 V) used in this study. The different behavior in perchloric as compared to sulphuric acid strongly suggests that the adsorption of spectator species from the electrolyte must play a role in the delay observed between the formation of CO_B/CO_M and that of CO_L in the potential region around 0.26 V, as does the fact that increasing the concentration of methanol results in a decrease (or even a cancellation in 0.1 M $HClO_4$ if the concentration is high enough) of the delay between the formation of the two CO_{ad} species (after all, the adsorption of methanol or a methanol-derived intermediate must necessarily be the first step of the dehydrogenation reaction). Furthermore, the fact that the delay starts after the most negative of the H_{upd} peak suggests that the preference for CO_B/CO_M observed around 0.26 V is connected to the concomitant desorption of hydrogen and adsorption of either OH (0.1 M $HClO_4$) or sulphate (0.1 M H_2SO_4) from (111)-oriented low-coordinated sites.

Although CO_L is slightly favored over CO_B/CO_M on Pt(111) sites,[48] exposure of Pt(100) to CO in UHV results in a single CO_B band at 1874 cm^{-1} at very low coverages.[49] Based on this, we suggest that, while at the most negative potentials both (111)- and (100)-oriented defect sites are active for methanol dehydrogenation, upon displacement around 0.15 V of H_{upd} on (111)-

oriented defects by either adsorbed OH (OH_{ad}, perchloric acid) or adsorbed sulphate (sulphuric acid) (see CVs in Fig. 1), these sites are blocked or partially blocked. The (100)-oriented sites become then the most active for methanol dehydrogenation, resulting in CO_B/CO_M being occupied first when the first CO_{ad} molecules are produced. When (100)-oriented sites are also blocked between 0.25 and 0.35 V upon displacement of H_{upd} from these sites by the corresponding spectator species (see CVs in Fig. 1), the delay between the formation of CO_B/CO_M and that of CO_L decreases and, in perchloric acid, eventually disappears, suggesting that a similar degree of blocking of (111)- and (100)-oriented defects have resulted in a situation similar to that initially found at the most negative potentials. The observation of a clear delay between the formation of CO_B/CO_M and that of CO_L in 0.1 M H_2SO_4 even at 0.46 V suggests that adsorbed sulphate is more efficient blocking (111) than (100) defect sites. This is probably connected with the match between the geometry of the sites and the molecular structure of sulphate, as sulphate can block three contiguous Pt atoms (which furthermore, is the minimum atomic ensemble required by the dehydrogenation reaction[23]) on a (111) defect site by adsorbing through three of its oxygen atoms, while on a (100) defect site adsorption of sulphate must occur through bonding of two of its oxygen atoms to two Pt atoms.

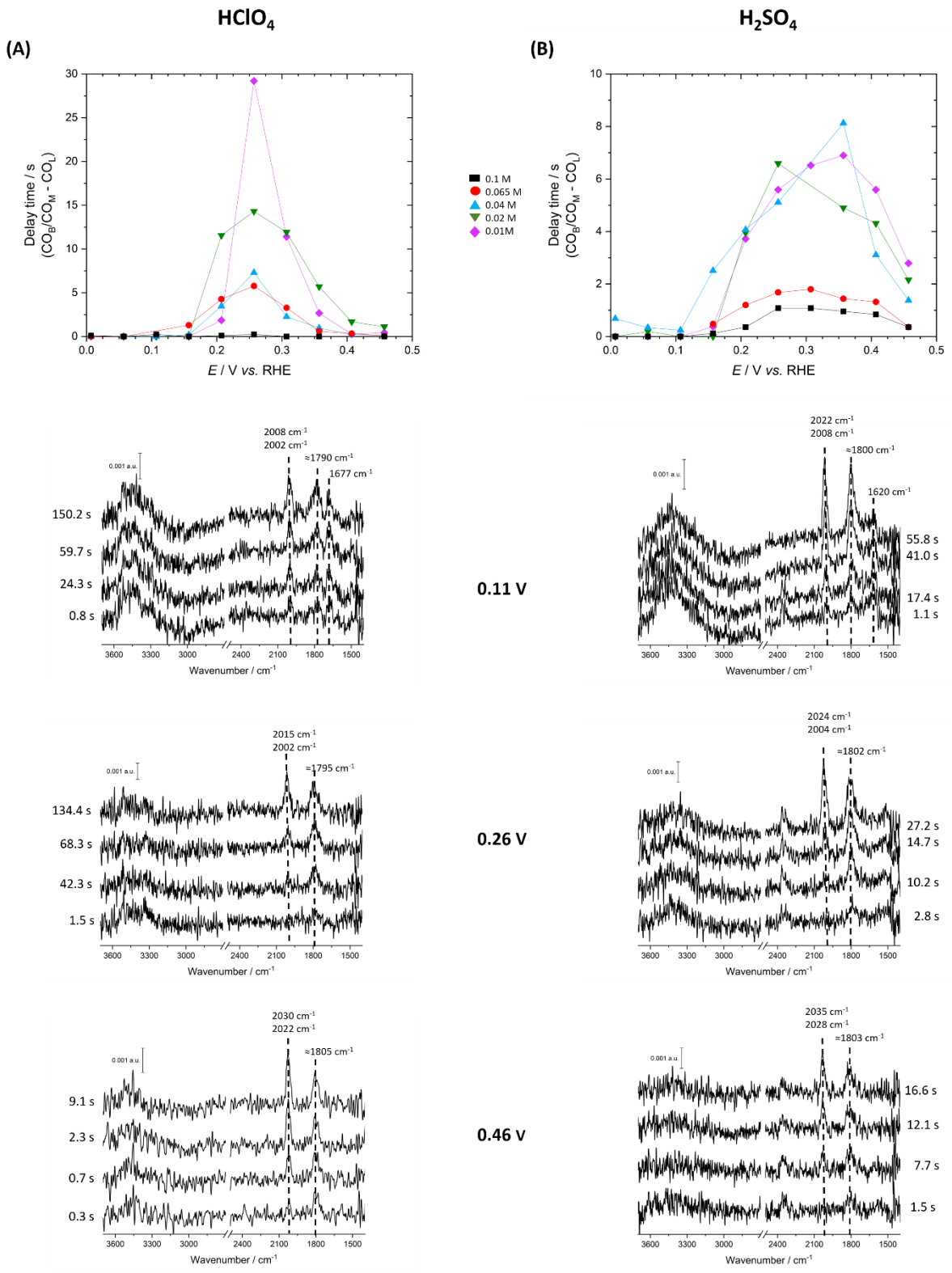

Figure 3. Top panel: Dependence on the applied potential of the delay between the first observation of a CO_B/CO_M band and that of CO_L in the presence of different concentrations of

methanol as follows: 0.01 M (purple rhombi), 0.02 M (inverted green triangles), 0.04 M (blue triangles), 0.065 M (red circles) and 0.1M (black squares) in 0.1 M $HClO_4$ **(A)** and 0.1 M H_2SO_4 **(B).** Lower panels: Selected individual spectra extracted from the corresponding time-resolved spectral series at specific times as indicated in the figure at 0.11 (first row), 0.26 (second row) and 0.46V (third row).

Another interesting feature in the spectra shown in Fig. 3 is the observation at the most negative potentials of a band at 1677 cm^{-1} (see, *e.g.*, spectra at $E = 0.11$ V in Fig. 3). This band, which is more intense in 0.1 M $HClO_4$ than in 0.1 M H_2SO_4, appears at too high a frequency to be attributable to the H-O-H bending mode of water. Actually, a smaller positive band around 1610 cm^{-1}, characteristic of interfacial water on a Pt electrode in this potential region,[50] can also be observed in the spectra. Jusys et al.[51] reported a similar band at 1660 cm^{-1} during the oxidation of formaldehyde on Pt in 0.5 M $HClO_4$ at $E \leq 0.1$ V and attributed it to adsorbed formyl (HCO_{ad}), which would be the intermediate in the oxidation of H_2CO to CO_{ad}. We, therefore, assign this band to HCO_{ad} on Pt, which must be the last intermediate in the dehydrogenation of methanol to CO_{ad}. Because the coverage by HCO_{ad} must correspond to a steady state in which its rate of formation equals its rate of oxidation to CO_{ad}, the fact that this species is observed only at the most negative potentials suggests that the rate of oxidation of HCO_{ad} to CO_{ad}, increases faster with potential than the rate of oxidation of methanol to HCO_{ad}. The smaller intensity of the HCO_{ad} band in 0.1 M H_2SO_4 is also consistent with the observation that in this potential region the rate of dehydrogenation of methanol is faster in sulphuric than in perchloric acid (see below).

3.2. Potential dependence of the rate of methanol dehydrogenation to CO_{ad}: Tafel plots. As discussed in the Introduction, infrared spectroscopy offers the possibility of analysing the rate at which CO_{ad} is formed (*i.e.*, the rate of the reaction) without any interference of other processes

by analysing the growth of the corresponding vibrational bands. It is well known that, due to depolarisation effects provoked by dipole-dipole coupling between neighbouring oscillators, the dependence of the integrated absorbance of CO_{ad} (I_{CO}) on θ_{CO} increasingly deviates from linearity with increasing coverage and, at high coverages, I_{CO} becomes insensitive to coverage or even starts decreasing with increasing coverage.[52] However, at sufficiently low coverage, the linearity between absorbance and coverage holds well and I_{CO_L} has often been used as a proxy for θ_{CO}.[37,53]

Fig.4 shows plots of the time evolution of I_{CO_L}, of $I_{CO_{B/CO_M}}$ and of their sum ($I_{CO_L} + I_{CO_{B/CO_M}}$), as well as of the time dependence of the corresponding derivatives with respect to time ($\frac{dI_{CO_L}}{dt}$, $\frac{dI_{CO_{B/CO_M}}}{dt}$ and $\frac{d(I_{CO_L}+I_{CO_{B/CO_M}})}{dt}$, respectively), obtained at 0.11, 0.26 and 0.46 V from a series of time-resolved ATR-SEIRA spectra in 0.1 M $HClO_4$ (Fig.4A) and 0.1 M H_2SO_4 (Fig.4B) containing 0.01 M methanol. As expected, at all the potentials and independently of the composition of the electrolyte, both I_{CO_L} and $I_{CO_{B/CO_M}}$ grow monotonically and then level off until eventually reaching a constant value when the maximum coverage possible is reached (see Fig.S3). Please note that, because a minimum of three contiguous Pt atoms is needed for the dehydrogenation reaction to proceed,[23] once a value of θ_{CO} has been reached at which these minimum atomic ensembles have disappeared from the surface, no more CO_{ad} can be formed, and the maximum θ_{CO} reached by methanol dehydrogenation is always lower than that achievable by direct adsorption of CO.

Because the product of the reaction (CO_{ad}) blocks sites on the surface, any kinetic study must be based on the rate of formation of CO_{ad} at $t = 0$, when all the surface is active. In cases in which

the CO_L band is dominant at all times, ignoring $I_{CO_{B/CO_M}}$ will not lead to any artefact when analysing the rate of the reaction.[47] However, in the particular case of methanol dehydrogenation, as we have shown in the previous section, precisely at the times relevant for the kinetic analysis (*i.e.*, when $t \to 0$), I_{CO_L} and $I_{CO_{B/CO_M}}$ are similar and, in some cases, CO_B/CO_M is the only band present in the spectra. Therefore, ignoring $I_{CO_{B/CO_M}}$ would lead to a serious underestimation of both θ_{CO} and the rate at which it increases (*i.e.*, of the reaction rate) in the initial stages of the reaction. This can be clearly seen in the results at 0.26 V reported in Fig. 4 (middle panel), where $\frac{dI_{CO_L}}{dt}$ (red line) is seen to initially increase until a maximum is reached, after which it slowly decays to zero. A similar maximum in the rate of methanol dehydrogenation was found by Liu *et al.*[25] when using I_{CO_L} as a proxy for θ_{CO} in a similar study, albeit focusing on more positive potentials and higher methanol concentrations than those used here. Using exclusively I_{CO_L} as a proxy for θ_{CO}, ignoring $I_{CO_{B/CO_M}}$, would lead to the extremely surprising and unlikely conclusion that blocking the Pt surface with CO_{ad} initially results in an activation of the surface, and only at higher coverage does CO_{ad} behave as a reaction inhibiting species. That this conclusion is wrong and is due to ignoring $I_{CO_{B/CO_M}}$ (black lines in Fig. 4) can be easily seen from its time evolution, which shows that, in the same time interval in which the formation of CO_L accelerates, that of CO_B/CO_M decelerates at the same rate or faster. When both CO_L and CO_B/CO_M are used to estimate q_{CO} and the rate at which it increases ($I_{CO_L} + I_{CO_{B/CO_M}}$ and $\frac{d(I_{CO_L}+I_{CO_{B/CO_M}})}{dt}$ in Fig. 4 (green lines), respectively), the much more reasonable conclusion that the reaction rate either remains initially constant and later slowly decays to zero or decays to zero from $t = 0$ is reached. The fact that, under certain conditions, the rate of the reaction is seen to initially remain constant for a relatively long time suggests that, during this time, θ_{CO} remains

low enough as to have a negligible blocking effect. In other words, it is a confirmation that we are analysing the kinetics of the reaction when θ_{CO} is extremely low.

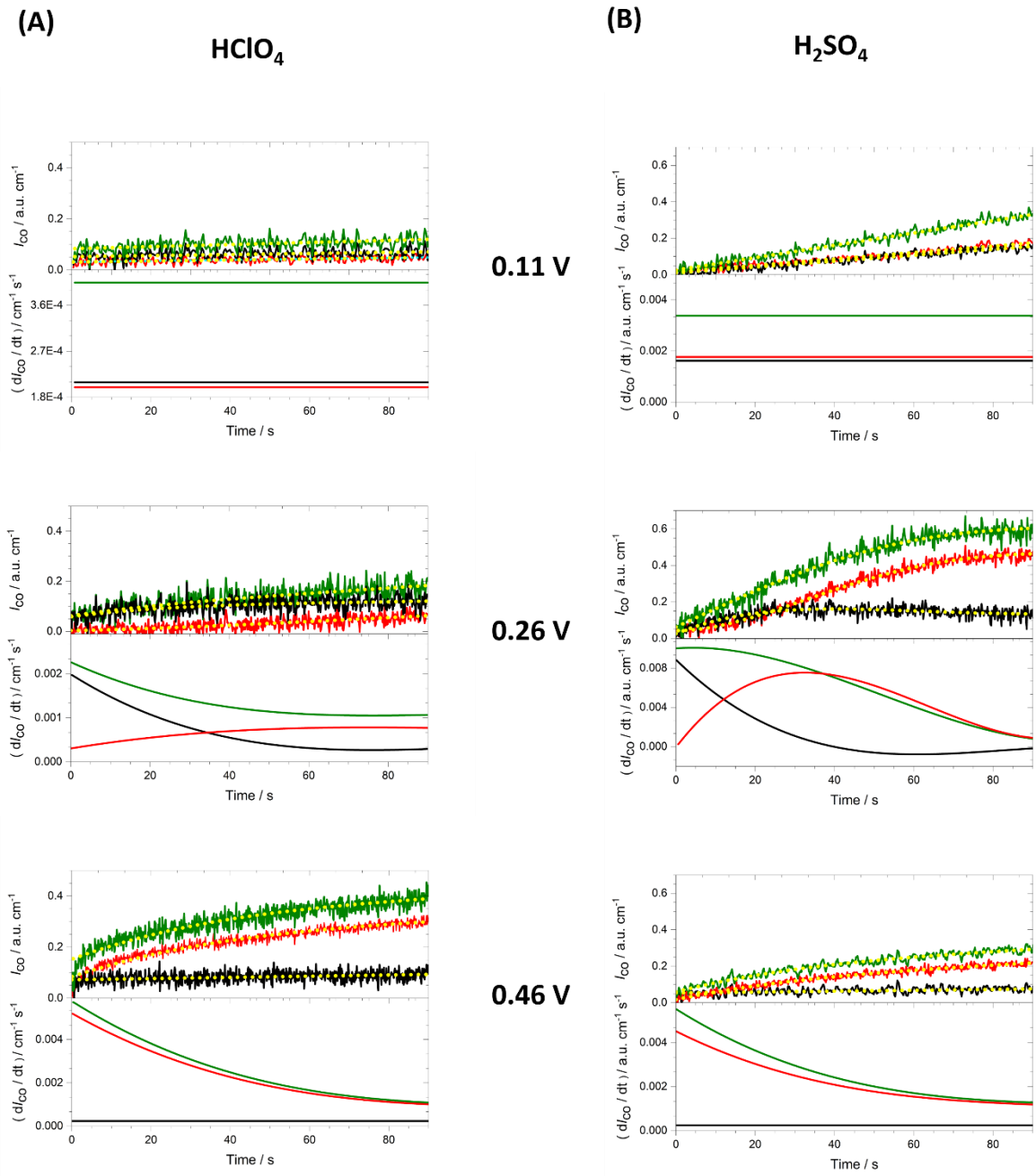

Figure 4. Time dependence of I_{CO_L} (red), $I_{CO_{B/CO_M}}$ (black) and $I_{CO_L} + I_{CO_{B/CO_M}}$ (green) (top panels) and of the corresponding derivatives with respect to time (lower panels) obtained from a

series of time-resolved ATR-SEIRA spectra in 0.1 M $HClO_4$ **(A)** and 0.1 M H_2SO_4 **(B)** containing 0.01 M CH_3OH, recorded after a potential step from 0.96 and 0.91 V, respectively, to 0.11 (top), 0.26 (middle) and 0.46 V (bottom). The integrated intensity vs. time data were smoothed using either a linear fit (data at 0.11 V) or a fit to a 4^{th} order polynomial (data at 0.26 and 0.46 V) and the result of the fit (dotted yellow lines) was used to obtain the derivatives in the bottom panels. The results of differentiating the raw integrated intensity *vs.* time curves without any further treatment (Fig.S4**)** and after smoothing the derivative using an average signal processing method (Fig.S5**)** are provided in the Supporting Information.

From analyses like that presented in Fig. 4 the intrinsic rate of formation of CO_{ad} (*i.e.*, the rate at $t = 0$, when no site-blocking CO_{ad} has been formed) can be extracted at each applied potential, which allows us to obtain Tafel plots of the applied potential *vs.* the logarithm of the rate of methanol dehydrogenation to CO_{ad}. Fig. 5 shows these Tafel plots in both 0.1M $HClO_4$, (Fig. 5A) and 0.1 M H_2S0_4 (Fig. 5B) for several methanol concentrations. As can be seen in Fig. 5, the concentration of methanol has essentially no effect on the potential dependence of the reaction rate.

The most striking feature in the Tafel plots of Fig. 5 is that at 0.21 V (0.1 M $HClO_4$) and 0.16 V (0.1 M H_2SO_4) the rate of the reaction stops increasing with increasingly positive potential, as would be expected for an oxidation and, instead, remains constant or, in 0.1 M H_2SO_4, even decreases with increasing potential. This behavior extends up to 0.26 V in 0.1 M $HClO_4$ and up to 0.36 V in 0.1 M H_2SO_4, and then the expected increase in reaction rate with increasingly positive potential is found again, although with Tafel slopes that are larger than at $E \leq 0.21$ V (0.1 M $HClO_4$) or $E \leq 0.16$ V (0.1 H_2SO_4). The stronger effect in 0.1 M H_2SO_4 is by itself strong evidence that this disruption in the expected dependence of the reaction rate on the potential is

due to the adsorption of spectator species (OH_{ad} in 0.1 M $HClO_4$ and adsorbed sulphate in 0.1 M H_2SO_4). The potential region in which this effect is observed roughly coincides with that in which a delay between the first observation of CO_B/CO_M and that of CO_L was also observed (see Fig. 3 and the corresponding discussion), which adds additional support to our conclusion that such delay is due to blocking of (111)-oriented defect sites when H_{upd} is displaced from those sites by either OH_{ad} (perchloric acid solutions) or adsorbed sulphate (sulphuric acid solutions). As argued above when describing the effect of the adsorption of spectator species on the delay observed between the formation of CO_B/CO_M and that of CO_L, we believe that the stronger deceleration of the increase of the reaction rate with increasingly positive potential in 0.1 M H_2SO_4 is due to the more efficient blocking of (111)-oriented defect sites by specifically adsorbed sulphate. Once H_{upd} starts desorbing from (100)-oriented sites, the reaction rate starts increasing with potential again, although with a larger Tafel slope (average of five concentrations, *ca.* 0.36 V ± 0.1 in perchloric acid and *ca.* 0.41 V ± 0.1 in sulphuric acid; similar values of the Tafel slope were found by Liu *et al.*,[25] whose study was restricted precisely to potentials above 0.30 V). We do not discard that oxidation of CO_{ad}, even if very slow (as hinted by the potential dependence of the CO_L stretching frequency, see below), contributes to the high Tafel slopes found in this potential region, particularly at the most positive potential.

Smaller Tafel slopes are found in the potential region below 0.26 V, *ca.* 0.11 V ± 0.01 in perchloric acid and 0.07 V ± 0.01 in sulfuric acid. Interestingly, in this potential region the Tafel slope is larger in 0.1 M $HClO_4$ than in 0.1 M H_2SO_4, which is exactly the opposite of the behaviour observed at the most positive potentials studied. It is reasonable to assume that sulphate adsorbs more strongly on Pt than OH because it can bond to the electrode surface through two or, on (111)-oriented sites, even three of its oxygen atoms. In this potential region,

H_{upd} on (111)-oriented defect sites is gradually replaced by either OH_{ad} or adsorbed sulphate, depending on the electrolyte used, and, initially, adsorption of sulphate through two or three oxygen atoms might not be possible simply because the corresponding sites have not been freed from H_{upd} yet. If adsorption of sulphate through only one of its oxygen atoms is slightly weaker than that of OH, access of methanol to the reactive sites in 0.1 M H_2SO_4 might be slightly easier than in 0.1 M $HClO_4$ and the gradual desorption of H_{upd} with increasing potential would lead to a larger increase of the reaction rate in the former than in the latter case. Once a potential is reached at which H_{upd} has desorbed from all the (111)-oriented defect sites and strong adsorption of sulphate through three of its oxygen atoms becomes possible, sulphate shows a stronger blocking effect, resulting in negative Tafel slopes, as we have discussed above.

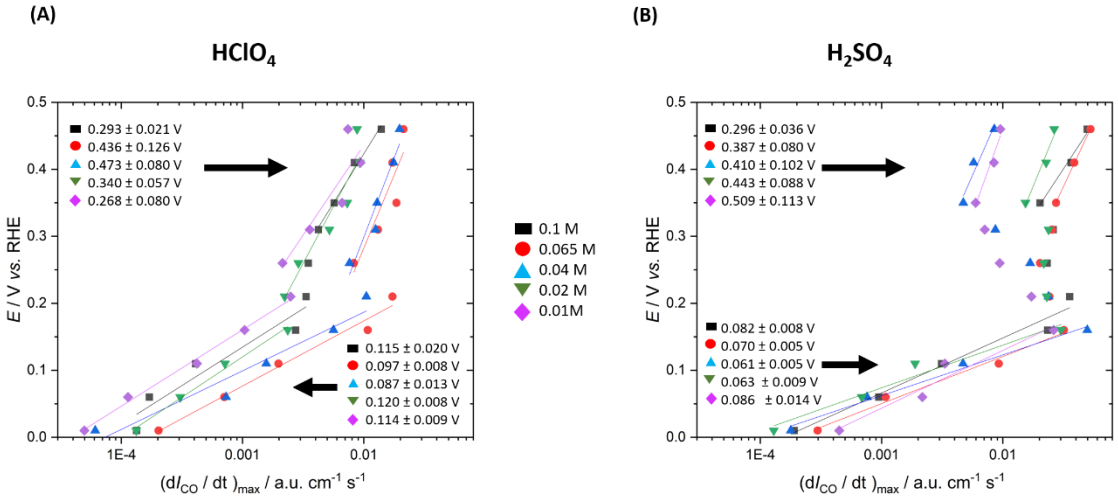

Figure 5. Tafel plots for the dehydrogenation of methanol to CO_{ad} on Pt in the potential region between 0.01V and 0.46 V in 0.1 M $HClO_4$ **(A)** and 0.1 M H_2S0_4 **(B)** in the presence of different concentrations of methanol, as follows: 0.01 M (purple rhombi), 0.02 M (inverted green triangles), 0.04 M (blue triangles), 0.065 M (red circles) and 0.1M (black squares).

We would like to finish this section with a brief word on the use of Tafel slopes to deduce reaction mechanisms of complex electrocatalytic reactions like the one dealt with in this work. Typically, Tafel slopes are assumed to describe the increase in the reaction rate due to the decrease in the reaction's activation energy with increasing overpotential. However, in complex electrocatalytic reactions, how much the overpotential needs to be increased to multiply the reaction rate by 10 (*i.e.*, the Tafel slope) will not be determined just by the overpotential-induced decrease of the activation energy. Instead, as shown here, other factors like the potential dependence of the number of available active sites per unit area will also contribute to the value of the Tafel slope. Under these conditions, using the Tafel slope to deduce the rate-determining steps and the sequence of reaction steps preceding it becomes extremely challenging, when not outright impossible.

3.3. Diffusion of CO_{ad} from the active sites towards the rest of the surface and singleton frequency of CO_{ad} on Pt. Because with increasing coverage the distance between oscillating CO_{ad} dipoles on the Pt surface must continually decrease, a continuous increase of the CO-stretching frequency should be observed in parallel with the continuous increase in integrated absorbance. However, as shown in Fig 6A, this is quite unexpectedly not the case (for the sake of clarity, only the evolution of the CO_L frequency is shown in Fig. 6A). Instead, in the initial stages of the reaction, the frequency grows in a staircase manner, in which periods of constant or nearly constant frequency are followed by a sharp rise in frequency and then by a new period of constant or nearly constant frequency. The expected continuous increase in stretching frequency with continuously increasing coverage is observed only at relatively high coverage.

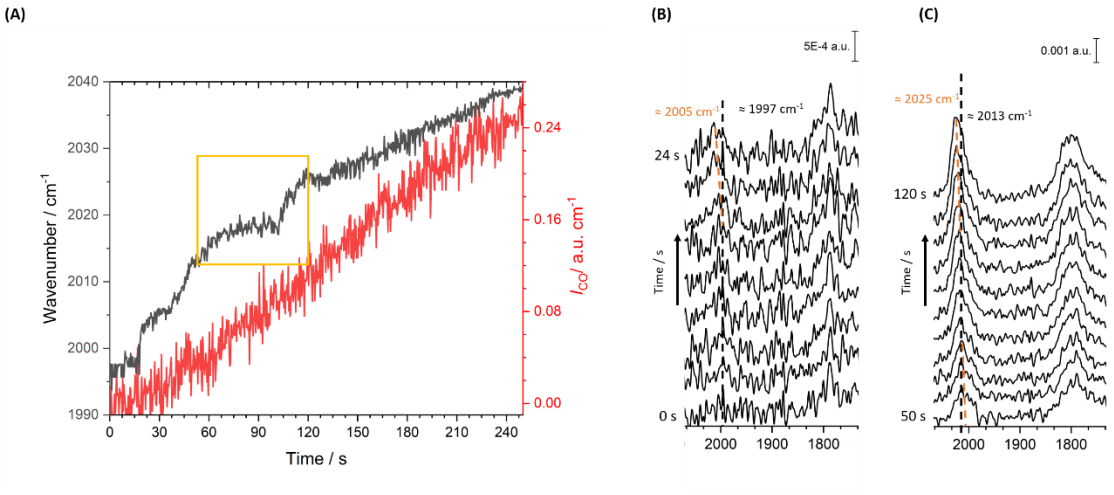

Figure 6. (A) Time evolution of the stretching frequency of CO_L (black line) and of I_{CO_L} (red line) obtained from a series of time-resolved ATR-SEIRA spectra of Pt in 0.1 M H_2SO_4 containing 0.01 M CH_3OH recorded after a potential step from 0.91 to 0.06 V vs. RHE. Individual spectra separated 3 s from each other and selected from the first 24 s are shown in **(B),** while spectra separated 7 s from each other and selected from the period between 50 and 120 s (yellow square in **A**) are shown in **(C).** Each spectrum consists of 2 interferograms recorded with 4 cm^{-1} spectral resolution, resulting in an interval between spectra of 0.4 s. The reference spectrum was recorded at 0.91 V.

The reason for this staircase behaviour can be found by analysing groups of spectra within individual periods of constant or nearly constant frequency. Fig. 6B shows that, in the first of these periods, corresponding to approximately the first 24 s of the reaction, in addition to a constant frequency, the CO_L band is symmetric and shows no evidence of inhomogeneous broadening. The constant frequency suggests that the growth in coverage is slow enough as to not result in dipole-dipole coupling, whereas the presence of a single, symmetric band, suggests that only one type of site is being occupied.[54,55] It is reasonable to assume that these sites are the most active ones for the dehydrogenation reaction, which, depending on the potential region and as discussed above,

must correspond to one-dimensional (111)- or (100)-oriented sites. The frequency at these initial stages of the reaction, 2002 cm^{-1} ± 2 between 0.01 and 0.06 V, must correspond to the singleton frequency of CO_L on those Pt step sites.[56] The sharp increase in frequency at around 20 s must correspond to the moment in which θ_{CO} in those specific sites has reached a threshold above which a further increase in coverage must necessarily lead to a rapidly decreasing average distance between CO_{ad} molecules. The fact that the sharp increase in frequency is followed by a new period of constant or nearly constant frequency suggests that the intermolecular repulsions associated with the increased coverage of these monodimensional sites provoke a spillover of the new CO_{ad} molecules formed into neighboring two-dimensional domains, where a larger number of adsorbates can be accommodated without a significant decrease in the average distance between them. This is confirmed by analysing one of the later periods of constant or nearly constant frequency, like the one shown in Fig. 6C. Now the band shows a clear inhomogeneous broadening, which suggests that, although the degree of dipole-dipole coupling is not increasing during this period, there exists coupling between CO_{ad} molecules at sites with similar but not identical stretching frequencies (*e.g.*, on step and on two-dimensional sites), which results in intensity being transferred from those molecules oscillating at lower frequencies (CO_{ad} on step sites) to those oscillating at higher frequencies (CO_{ad} on two-dimensional domains). The presence of several of these periods of constant or near-constant frequency suggests that there is more than one configuration of CO_{ad} on those two-dimensional domains in which the average distance between adsorbates can be kept nearly constant despite a slow but continuous increase in coverage.

Finally, we have analysed the potential dependence of the singleton frequency. Fig.7 shows the potential dependence of the CO_L frequency when $\theta_{CO} \rightarrow 0$ (Fig. 7A) and at the maximum coverage attainable through the dehydrogenation of methanol (Fig. 7B; due to the presence of a

CO_M and a CO_B band in the CO_B/CO_M feature, the analysis of its potential dependence at high coverage is not straightforward and has therefore not been included). Once the final coverage has been reached, the typical linear dependence with a slope of 33 cm^{-1} V^{-1} is observed,[46] although at around 0.3 V the potential dependence of the CO_L frequency levels off (Fig. 7B). This most likely signals a slight decrease in the maximum achievable θ_{CO} due the onset of CO_{ad} oxidation, as a decrease in dipole-dipole coupling will offset the potential-induced increase of the CO_L stretching frequency.

The singleton frequency displays, however, a completely different behaviour, with a very small dependence on potential which increases above 0.3 V (Fig. 7A) .The same potential dependence is found in $HClO_4$ (Fig. S6). We suggest that the smaller dependence on potential at the most negative potentials might be due to the presence of co-adsorbed H_{upd}, which at 0.30 V has nearly completely desorbed. An effect of co-adsorbed hydrogen on the magnitude of the Stark effect of linearly adsorbed cyanide and of CO_L on Pt(111) has been suggested before, although admittedly with the opposite effect of increasing the dependence of the frequency on the applied potential.[57]

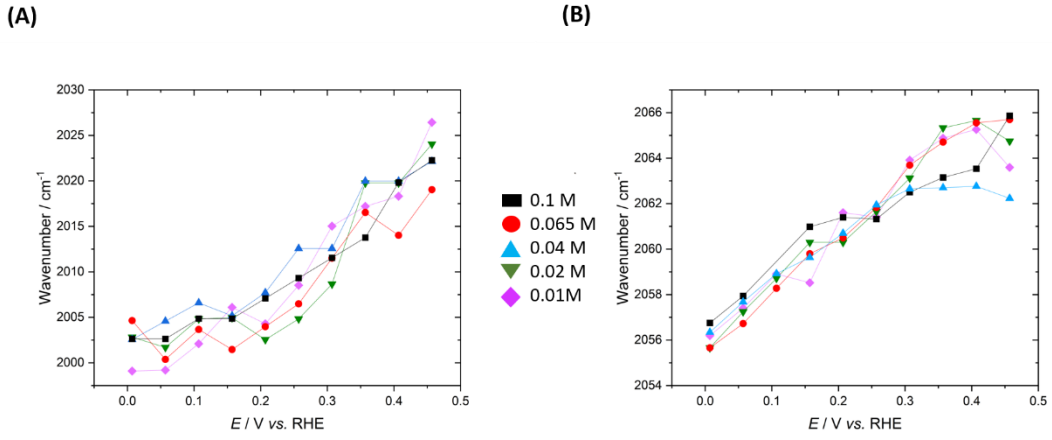

Figure 7. Potential dependence of the C-O stretching frequency of linearly-bonded CO_{ad} at the $\theta_{CO} \rightarrow 0$ limit **(A)** and when the maximum CO coverage has been reached **(B)** from a series of

time-resolved ATR-SEIRA spectra after a potential step from 0.91 V in 0.1 M H_2SO_4 containing CH_3OH at the following concentrations: 0.01 M (purple rhombi), 0.02 M (inverted green triangles), 0.04 M (blue triangles), 0.065 M (red circles) and 0.1M (black square).

4. CONCLUSIONS

The high sensitivity and the absence of transport limitations characteristic of ATR-SEIRAS, has enabled us to perform a detailed, real-time, analysis of the electrocatalytic dehydrogenation of methanol on platinum to CO_{ad} based on time-resolved spectra recorded simultaneously to current transients after a potential step.

Our results confirm previous reports that the reaction proceeds essentially on defect sites and that bidimensional domains (particularly those with (111) orientation) show little if any activity. However, based on the discontinuity observed in the potential dependence of the rate of oxidation of methanol to CO_{ad}, which coincides with the displacement of H_{upd} from (111)-oriented defect sites by either adsorbed OH (perchloric acid solutions) or adsorbed sulphate (sulphuric acid solutions), we conclude that the most active sites for the formation of CO_{ad} are (111) defect sites. The fact that, in the same potential region where this discontinuity occurs, formation of CO_B/CO_M precedes that of CO_L provides additional support to this conclusion. Clear differences in both the discontinuity in the Tafel plots and in the time elapsed between the first observation of CO_B/CO_M and that of CO_L when comparing experiments in 0.1 M $HClO_4$ with experiments in 0.1 M H_2SO_4 are evidence of the role played by spectator species in determining the rate of the reaction. A detailed comparative analysis of the evolution of the CO_L frequency and the integrated intensity of the corresponding band as the reaction proceeds reveals that there is a successive population of sites, whereby CO_{ad} diffuses from the most active sites,

which are populated first, into neighbouring bidimensional domains once the CO coverage on the active defect sites reaches a threshold value. We have also been able to identify adsorbed formyl as the last intermediate in the oxidation of methanol to CO_{ad}.

ASSOCIATED CONTENT

Supporting Information. Supporting Information containing the cyclic voltammograms at 0.1 V s^{-1} of a polycrystalline Pt electrode in 0.1 M H_2SO_4 and 0.1 M $HClO_4$ (Fig. S1), current transients after a potential step in methanol-free 0.1 M H_2SO_4 (Fig. S2), Table S1 with the exact times for the first observation of a CO_{ad} after a potential step; the evolution of the integrated intensity of the infrared bands over the whole duration of the experiment (Fig. S3), and the raw data in Fig. 4 without any data processing (Fig. S4) and after smoothing the time derivative of the integrated intensity of the infrared bands using an adjacent signal averaging method (Fig. S5) is available free of charge.

AUTHOR INFORMATION

Corresponding Author

*angel.cuestaciscar@abdn.ac.uk

Present Addresses

†School of Chemistry, Joseph Black Building-David Brewster Road, University of Edinburgh, EH9 3FJ, Edinburgh, UK.

Author Contributions

The manuscript was written through contributions of all authors. All authors have given approval to the final version of the manuscript.

Notes

The authors declare no competing financial interest.

ACKNOWLEDGMENT

L.P.-M. acknowledges a doctoral scholarship within the Leverhulme Centre for Doctoral Training in Sustainable Production of Chemicals and Materials (Grant DS-2017-073).

REFERENCES

(1) Parsons, R.; VanderNoot, T. The Oxidation of Small Organic Molecules. A Survey of Recent Fuel Cell Related Research. *J. Electroanal. Chem.* **1988**, *257*, 9–45.

(2) Love, J. G.; Brooksby, P. A.; McQuillan, A. J. Infrared Spectroelectrochemistry of the Oxidation of Absolute Methanol at a Platinum Electrode. *J. Electroanal. Chem.* **1998**, *464*, 99–100.

(3) González, M. J.; Hable, C. T.; Wrighton, M. S. Electrocatalytic Oxidation of Small Carbohydrate Fuels at Pt-Sn Modified Electrodes. *J. Phys. Chem. B* **1998**, *102*, 9881–9890.

(4) Koper, M. T. M.; Lai, S. C. S.; Herrero, E. Mechanisms of the Oxidation of Carbon Monoxide and Small Organic Molecules at Metal Electrodes. In *Fuel Cell Catalysis: A Surface Science Approach*; Koper, M. T. M., Ed.; John Wiley & Sons: Hoboken, New Jersey, 2008; pp 159–207.

(5) Bagotzky, V. S.; Vassilyev, Y. B. Mechanism of Electro-Oxidation of Methanol on the Platinum Electrode. *Electrochim. Acta* **1967**, *12*, 1323–1343.

(6) Wasmus, S.; Wang, J. -T.; Savinell, R. F. Real-Time Mass Spectrometric Investigation of the Methanol Oxidation in a Direct Methanol Fuel Cell. *J. Electrochem. Soc.* **1995**, *142*, 3825–3833.

(7) Lin, W. -F.; Wang, J. -T.; Savinell, R. F. On-Line FTIR Spectroscopic Investigations of Methanol Oxidation in a Direct Methanol Fuel Cell. *J. Electrochem. Soc.* **1997**, *144*, 1917–1922.

(8) Hamnett, A. Mechanism and Electrocatalysis in the Direct Methanol Fuel Cell. *Catal. Today* **1997**, *38*, 445–457.

(9) Aricò, A. S.; Srinivasan, S.; Antonucci, V. DMFCs: From Fundamental Aspects to Technology Development. *Fuel Cells* **2001**, *1*, 133–161.

(10) Breiter, M. W. Comparative Voltammetric Study of Methanol Oxidation and Adsorption on Noble Metal Electrodes in Perchloric Acid Solutions. *Electrochim. Acta* **1963**, *8*, 973–983.

(11) Kua, J.; Goddard, W. A. Oxidation of Methanol on 2nd and 3rd Row Group VIII Transition Metals (Pt, Ir, Os, Pd, Rh, and Ru): Application to Direct Methanol Fuel Cells. *J. Am. Chem. Soc.* **1999**, *121*, 10928–10941.

(12) Herrero, E.; Chrzanowski, W.; Wieckowski, A. Dual Path Mechanism in Methanol Electrooxidation on a Platinum Electrode. *J. Phys. Chem.* **1995**, *99*, 10423–10424.

(13) B.Beden; C.Lamy; A.Bewick; K.Kunimatsu. Electrosorption of Methanol on a Platinnum Electrode. IR Spectroscopic Evidence for Adsrobed CO Species. *J. Electroanal. Chem.* **1981**, *121*, 343–347.

(14) Lin, W. F.; Zei, M. S.; Eiswirth, M.; Ertl, G.; Iwasita, T.; Vielstich, W. Electrocatalytic Activity of Ru-Modified Pt(111) Electrodes toward CO Oxidation. *J. Phys. Chem. B* **1999**, *103*, 6968–6977.

(15) Krausa, M.; Vielstich, W. Study of the Electrocatalytic Influence of Pt/Ru and Ru on the Oxidation of Residues of Small Organic Molecules. *J. Electroanal. Chem.* **1994**, *379*, 307–314.

(16) Ianniello, R.; Schmidt, V. M.; Stimming, U.; Stumper, J.; Wallau, A. CO Adsorption and Oxidation on Pt and PtRu Alloys: Dependence on Substrate Composition. *Electrochim. Acta* **1994**, *39*, 1863–1869.

(17) Shin, J.; Korzeniewski, C. Infrared Spectroscopic Detection of CO Formed at Step and Terrace Sites on a Corrugated Electrode Surface Plane during Methanol Oxidation. *J. Phys. Chem.* **1995**, *99*, 3419–3422.

(18) Housmans, T. H. M.; Koper, M. T. M. Methanol Oxidation on Stepped Pt[n(111) × (110)] Electrodes: A Chronoamperometric Study. *J. Phys. Chem. B* **2003**, *107*, 8557–8567.

(19) Grozovski, V.; Climent, V.; Herrero, E.; Feliu, J. M. The Role of the Surface Structure in the Oxidation Mechanism of Methanol. *J. Electroanal. Chem.* **2011**, *662*, 43–51.

(20) Herrero, E.; Franaszczuk, K.; Wieckowski, A. Electrochemistry of Methanol at Low Index Crystal Planes of Platinum. An Integrated Voltammetric and Chronoamperometric Study. *J. Phys. Chem.* **1994**, *98*, 5074–5083.

(21) Housmans, T. H. M.; Wonders, A. H.; Koper, M. T. M. Structure Sensitivity of Methanol Electrooxidation Pathways on Platinum: An on-Line Electrochemical Mass Spectrometry Study. *J. Phys. Chem. B* **2006**, *110*, 10021–10031.

(22) K.D.Gibson; L.H.Dubois. Step Effects in the Thermal Decomposition of Methanol on Pt(111). *Surf. Sci.* **1990**, *233*, 59–64.

(23) Cuesta, A. At Least Three Contiguous Atoms Are Necessary for CO Formation during Methanol Electrooxidation on Platinum. *J. Am. Chem. Soc.* **2006**, *128*, 13332–13333.

(24) Cuesta, A.; Escudero, M.; Lanova, B.; Baltruschat, H. Cyclic Voltammetry, FTIRS, and DEMS Study of the Electrooxidation of Carbon Monoxide, Formic Acid, and Methanol on Cyanide-Modified Pt(111) Electrodes. *Langmuir* **2009**, *25*, 6500–6507.

(25) Liu, S. X.; Liao, L. W.; Tao, Q.; Chen, Y. X.; Ye, S. The Kinetics of CO Pathway in Methanol Oxidation at Pt Electrodes, a Quantitative Study by ATR-FTIR Spectroscopy. *Phys. Chem. Chem. Phys.* **2011**, *13*, 9725–9735.

(26) Greeley, J.; Mavrikakis, M. A First-Principles Study of Methanol Decomposition on Pt(111). *J. Am. Chem. Soc.* **2002**, *124*, 7193–7201.

(27) Lebedeva, N. P.; Rodes, A.; Feliu, J. M.; Koper, M. T. M.; Van Santen, R. A. Role of Crystalline Defects in Electrocatalysis: CO Adsorption and Oxidation on Stepped Platinum Electrodes as Studied by in Situ Infrared Spectroscopy. *J. Phys. Chem. B* **2002**, *106*, 9863–9872.

(28) Van Der Niet, M. J. T. C.; Garcia-Araez, N.; Hernández, J.; Feliu, J. M.; Koper, M. T. M. Water Dissociation on Well-Defined Platinum Surfaces: The Electrochemical Perspective. *Catal. Today* **2013**, *202*, 105–113.

(29) Climent, V.; Gómez, R.; Orts, J. M.; Feliu, J. M. Thermodynamic Analysis of the Temperature Dependence of OH Adsorption on Pt(111) and Pt(100) Electrodes in Acidic Media in the Absence of Specific Anion Adsorption. *J. Phys. Chem. B* **2006**, *110*, 11344–11351.

(30) Mukouyama, Y.; Kikuchi, M.; Samjeské, G.; Osawa, M.; Okamoto, H. Potential Oscillations in Galvanostatic Electrooxidation of Formic Acid on Platinum: A Mathematical Modeling and Simulation. *J. Phys. Chem. B* **2006**, *110*, 11912–11917.

(31) Samjeské, G.; Miki, A.; Osawa, M. Electrocatalytic Oxidation of Formaldehyde on Platinum under Galvanostatic and Potential Sweep Conditions Studied by Time-Resolved Surface-Enhanced Infrared Spectroscopy. *J. Phys. Chem. C* **2007**, *111*, 15074–15083.

(32) Cuesta, A.; Cabello, G.; Osawa, M.; Gutiérrez, C. Mechanism of the Electrocatalytic Oxidation of Formic Acid on Metals. *ACS Catal.* **2012**, *2*, 728–738.

(33) Cuesta, A.; Cabello, G.; Gutiérrez, C.; Osawa, M. Adsorbed Formate: The Key Intermediate in the Oxidation of Formic Acid on Platinum Electrodes. *Phys. Chem. Chem. Phys.* **2011**, *13*, 20091–20095.

(34) Cuesta, A.; Cabello, G.; Hartl, F. W.; Escudero-Escribano, M.; Vaz-Domínguez, C.; Kibler, L. A.; Osawa, M.; Gutiérrez, C. Electrooxidation of Formic Acid on Gold: An ATR-SEIRAS Study of the Role of Adsorbed Formate. *Catal. Today* **2013**, *202*, 79–86.

(35) Chen, Y. X.; Miki, A.; Ye, S.; Sakai, H.; Osawa, M. Formate, an Active Intermediate for Direct Oxidation of Methanol on Pt Electrode. *J. Am. Chem. Soc.* **2003**, *125*, 3680–3681.

(36) Zhu, Y.; Uchida, H.; Yajima, T.; Watanabe, M. Attenuated Total Reflection-Fourier Transform Infrared Study of Methanol Oxidation on Sputtered Pt Film Electrode. *Langmuir* **2001**, *17*, 146–154.

(37) K.Kunimatsu; H.Kita. Infrared Spectroscopic Study of Methanol and Formic Acid Adsorbates on a Platinum Electrode. Part II. Role of the Linear CO(a) Derived from Methanol and Formic Acid in the Electrocatalytic Oxidation of CH3OH and HCOOH. *J. Electroanal. Chem.* **1897**, *155–172*, 2001–2002.

(38) Miki, A.; Ye, S.; Osawa, M. Surface-Enhanced IR Absorption on Platinum Nanoparticles: An Application to Real-Time Monitoring of Electrocatalytic Reactions. *Chem. Commun.* **2002**, *2* (14), 1500–1501.

(39) Yan, Y. G.; Yang, Y. Y.; Peng, B.; Malkhandi, S.; Bund, A.; Stimming, U.; Cai, W. Bin. Study of CO Oxidation on Polycrystalline Pt Electrodes in Acidic Solution by ATR-SEIRAS. *J. Phys. Chem. C* **2011**, *115*, 16378–16388.

(40) Shiroishi, H.; Ayato, Y.; Kunimatsu, K.; Okada, T. Study of Adsorbed Water on Pt during Methanol Oxidation by ATR-SEIRAS (Surface-Enhanced Infrared Absorption Spectroscopy). *J. Electroanal. Chem.* **2005**, *581*, 132–138.

(41) Yoshimi, K.; Song, M. B.; Ito, M. Carbon Monoxide Oxidation on a Pt(111) Electrode Studied by in-Situ IRAS and STM: Coadsorption of CO with Water on Pt(111). *Surf. Sci.* **1996**, *368*, 389–395.

(42) Samjeské, G.; Komatsu, K. I.; Osawa, M. Dynamics of CO Oxidation on a Polycrystalline Platinum Electrode: A Time-Resolved Infrared Study. *J. Phys. Chem. C* **2009**, *113*, 10222–10228.

(43) Cuesta, A.; Shiroishi, H.; Ayato, Y.; Kunimatsu, K.; Okada, T. Comments on the Paper by H. Shiroishi, Y. Ayato, K. Kunimatsu and T. Okada Entitled "Study of Adsorbed Water on Pt during Methanol Oxidation by ATR-SEIRAS (Surface-Enhanced Infrared Absorption Spectroscopy)" [J. Electroanal. Chem. 581 (2005) 132]. *J. Electroanal. Chem.* **2006**, *587*, 329–330.

(44) Chang, S. C.; Weaver, M. J. Coverage- and Potential-Dependent Binding Geometries of Carbon Monoxide at Ordered Low-Index Platinum- and Rhodium-Aqueous Interfaces: Comparisons with Adsorption in Corresponding Metal-Vacuum Environments. *Surf. Sci.* **1990**, *238*, 142–162.

(45) Heinen, M.; Chen, Y. X.; Jusys, Z.; Behm, R. J. CO Adsorption Kinetics and Adlayer Build-up Studied by Combined ATR-FTIR Spectroscopy and on-Line DEMS under Continuous Flow Conditions. *Electrochim. Acta* **2007**, *53*, 1279–1289.

(46) Kim, C. S.; Tornquist, W. J.; Korzeniewski, C. Infrared Spectroscopy as a Probe of CO Adsorption at Pt(335) under Aqueous Electrochemical Conditions. *J. Phys. Chem.* **1993**, *97*, 6484–6491.

(47) Silva, C. D.; Cabello, G.; Christinelli, W. A.; Pereira, E. C.; Cuesta, A. Simultaneous Time-Resolved ATR-SEIRAS and CO-Charge Displacement Experiments: The Dynamics of CO Adsorption on Polycrystalline Pt. *J. Electroanal. Chem.* **2017**, *800*, 25–31.

(48) Tüshaus, M.; Schweizer, E.; Hollins, P.; Bradshaw, A. M. Yet Another Vibrational Study of the Adsorption System Pt{111}-CO. *J. Electron Spectros. Relat. Phenomena* **1987**, *44*, 305–316.

(49) Martin, R.; Gardner, P.; Bradshaw, A. M. The Adsorbate-Induced Removal of the Pt{100} Surface Reconstruction. Part II: CO. *Surf. Sci.* **1995**, *342*, 69–84.

(50) Osawa, M.; Tsushima, M.; Mogami, H.; Samjeské, G.; Yamakata, A. Structure of Water at the Electrified Platinum-Water Interface: A Study by Surface-Enhanced Infrared Absorption Spectroscopy. *J. Phys. Chem. C* **2008**, *112*, 4248–4256.

(51) Jusys, Z.; Behm, R. J. Adsorption and Oxidation of Formaldehyde on a Polycrystalline Pt Film Electrode: An in Situ IR Spectroscopy Search for Adsorbed Reaction Intermediates. *Beilstein J. Nanotechnol.* **2014**, *5*, 747–759.

(52) Borguet, E.; Dai, H. L. Site-Specific Properties and Dynamical Dipole Coupling of CO Molecules Adsorbed on a Vicinal Cu(100) Surface. *J. Chem. Phys.* **1994**, *101*, 9080–9095.

(53) Liao, L. W.; Liu, S. X.; Tao, Q.; Geng, B.; Zhang, P.; Wang, C. M.; Chen, Y. X.; Ye, S. A Method for Kinetic Study of Methanol Oxidation at Pt Electrodes by Electrochemical in Situ Infrared Spectroscopy. *J. Electroanal. Chem.* **2011**, *650*, 233–240.

(54) Hollins, P. The Influence of Surface Defects on the Infrared Spectra of Adsorbed Species. *Surf. Sci. Rep.* **1992**, *16*, 51–94.

(55) Hollins, P.; Pritchard, J. Infrared Studies of Chemisorbed Layers on Single Crystals. *Prog. Surf. Sci.* **1985**, *19*, 275–349.

(56) Severson, M. W.; Stuhlmann, C.; Villegas, I.; Weaver, M. J. Dipole-Dipole Coupling Effects upon Infrared Spectroscopy of Compressed Electrochemical Adlayers: Application to the Pt(111)/CO System. *J. Chem. Phys.* **1995**, *103*, 9832–9843.

(57) Cuesta, A.; Escudero, M.; Lanova, B.; Baltruschat, H. Cyclic Voltammetry, FTIRS, and DEMS Study of the Electrooxidation of Carbon Monoxide, Formic Acid, and Methanol on Cyanide-Modified Pt(111) Electrodes. *Langmuir* **2009**, *25*, 6500–6507.

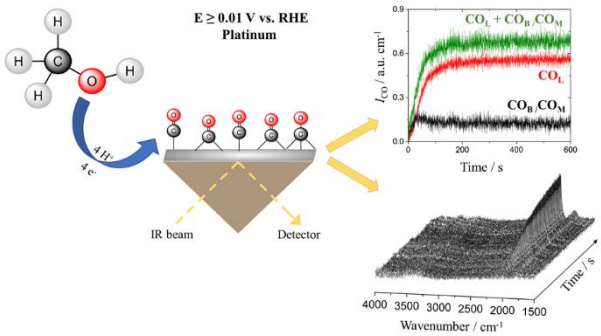

For Table of Contents Only

SUPPORTING INFORMATION

Methanol Dehydrogenation on Pt Electrodes: Active Sites and Role of Adsorbed Spectators Revealed through Time-Resolved ATR-SEIRAS

Laura Pérez-Martínez, Laura M. Machado de los Toyos,† Jani J. Shibuya, and Angel Cuesta.*

School of Natural and Computing Sciences, University of Aberdeen, Aberdeen AB24 3UE, Scotland, UK

†Current address: School of Chemistry, Joseph Black Building-David Brewster Road, University of Edinburgh, EH9 3FJ, Edinburgh, UK

*Corresponding author: angel.cuestaciscar@abdn.ac.uk

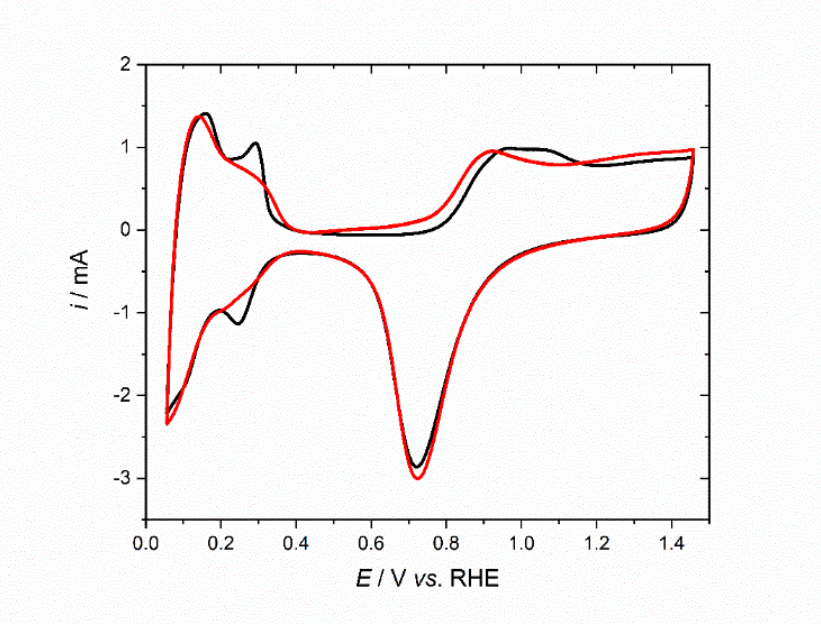

Figure S1.Cyclic voltammogram at 0.1 V $s^{-1}$of a polycrystalline Pt electrode in 0.1 M H_2SO_4 (red) and 0.1 M $HClO_4$ (black). The difference in the current intensity between both CVs is because two different Pt films were used.

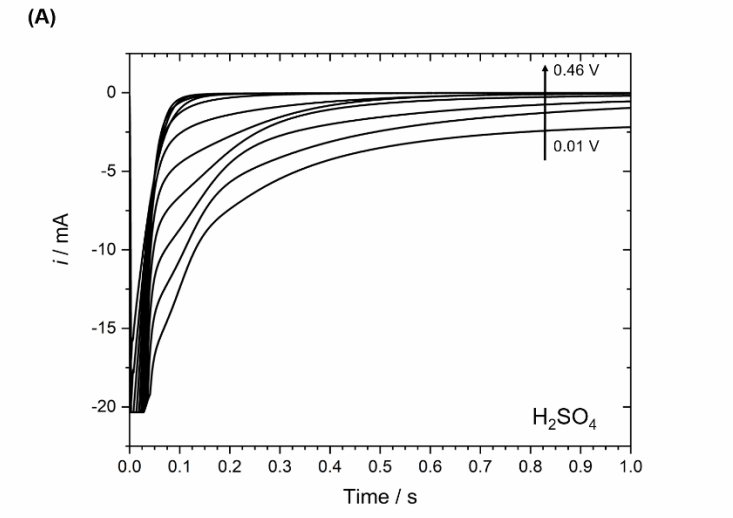

Figure S2. Characteristic current transients of a Pt thin film deposited on Si in methanol-free 0.1 M H_2SO_4 after a potential step from 0.91 V to a potential between 0.01 and 0.46 V (potentil

increases in 0.05 V steps between each transient). Similar transients were recorded in 0.1 M $HClO_4$ for steps from 0.96 V to the same final potentials.

Table S1. Specific times after the potential step from 0.91 V in presence of 0.1 M H_2SO_4 to the corresponding sample potential in each figure at which the first CO_{ad} band was observed after the potential step.

Figure number		**Time at which the first CO_{ad} band is observed / s**
2	0.16 V	2
3		
	A) $HClO_4$ 0.1 M	
	0.11 V	1.8
	0.26 V	1.5
	0.46 V	0.6
	B) H_2SO_4 0.1M	
	0.11 V	1.2
	0.26 V	1.5
	0.46 V	2.2
6	0.06 V	23.8

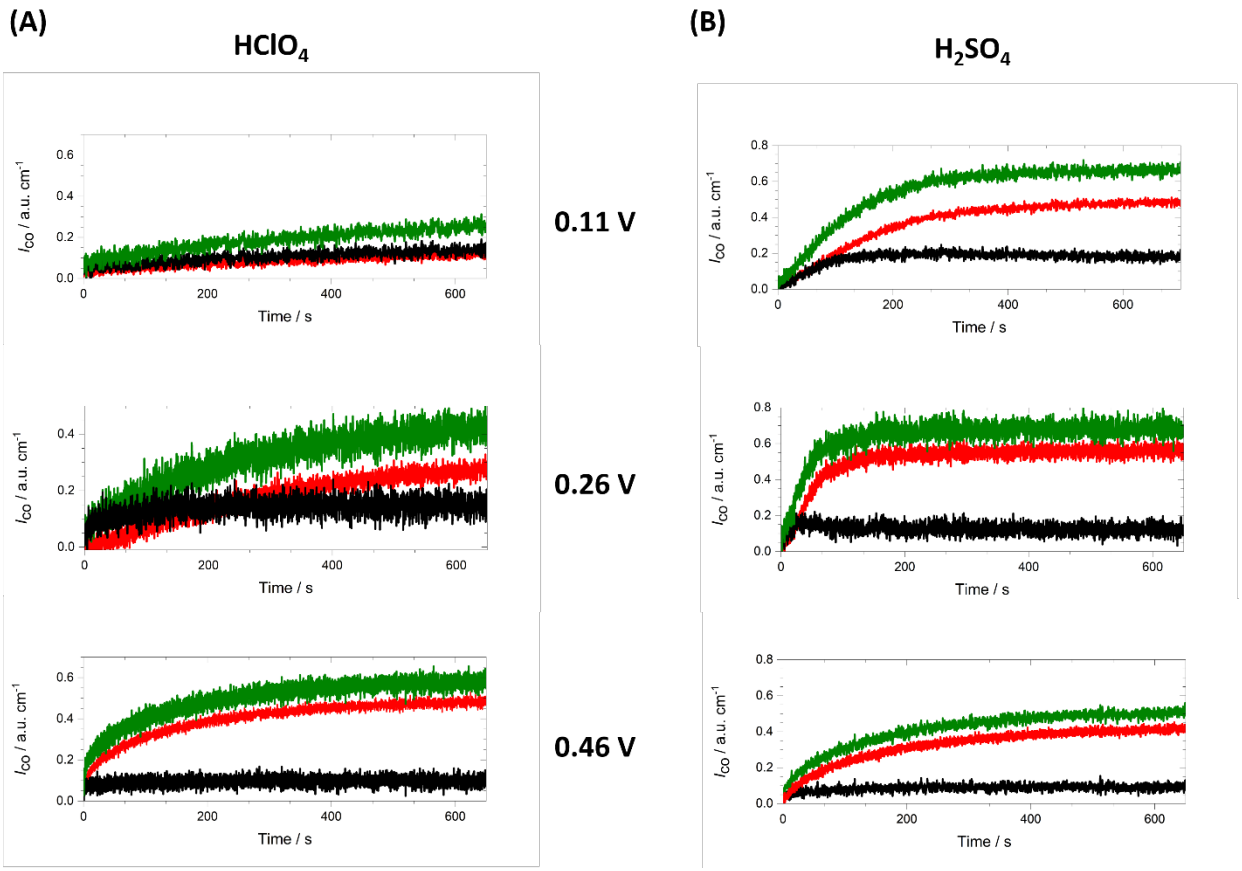

Figure S3. Time dependence over the whole duration of the current transient of I_{CO_L} (red), I_{CO_B/CO_M} (black) and $I_{CO_L} + I_{CO_B/CO_M}$ (green) obtained from a series of time-resolved ATR-SEIRA spectra in 0.1 M $HClO_4$ **(A)** and 0.1 M H_2SO_4 **(B)** containing 0.01 M CH_3OH, recorded after a potential step from 0.96 and 0.91 V, respectively, to 0.11 (top), 0.26 (middle) and 0.46 (bottom) V.

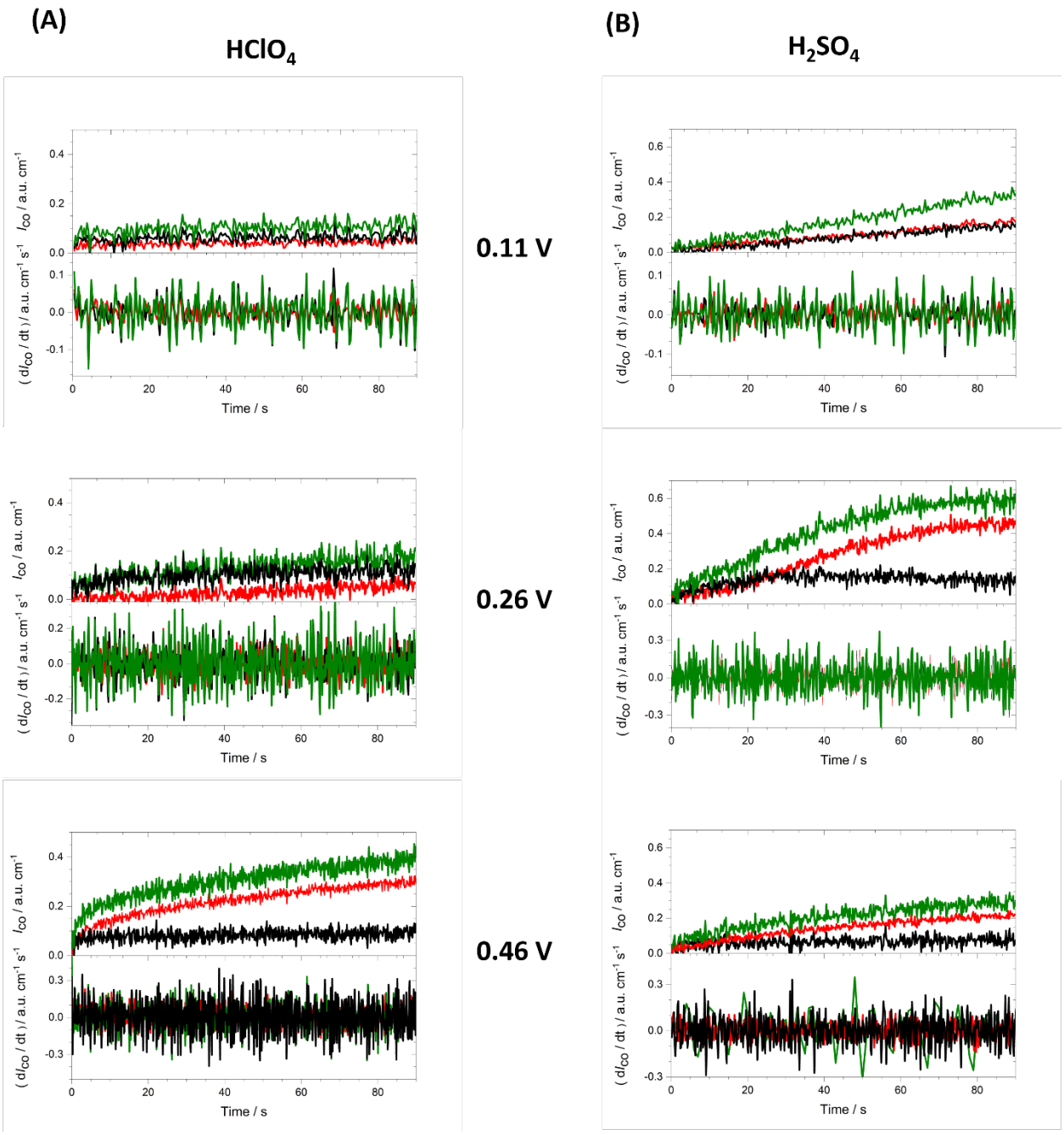

Figure S4.Time dependence of I_{CO_L} (red), I_{CO_B/CO_M} (black) and $I_{CO_L} + I_{CO_B/CO_M}$ (green) (top panels) and of the derivatives of the corresponding raw, unsmoothed data with respect to time (lower panels) obtained from a series of time-resolved ATR-SEIRA spectra in 0.1 M $HClO_4$ **(A)** and 0.1 M H_2SO_4 **(B)** containing 0.01 M CH_3OH, recorded after a potential step from 0.96 and 0.91 V, respectively, to 0.11 (top), 0.26 (middle) and 0.46 (bottom) V

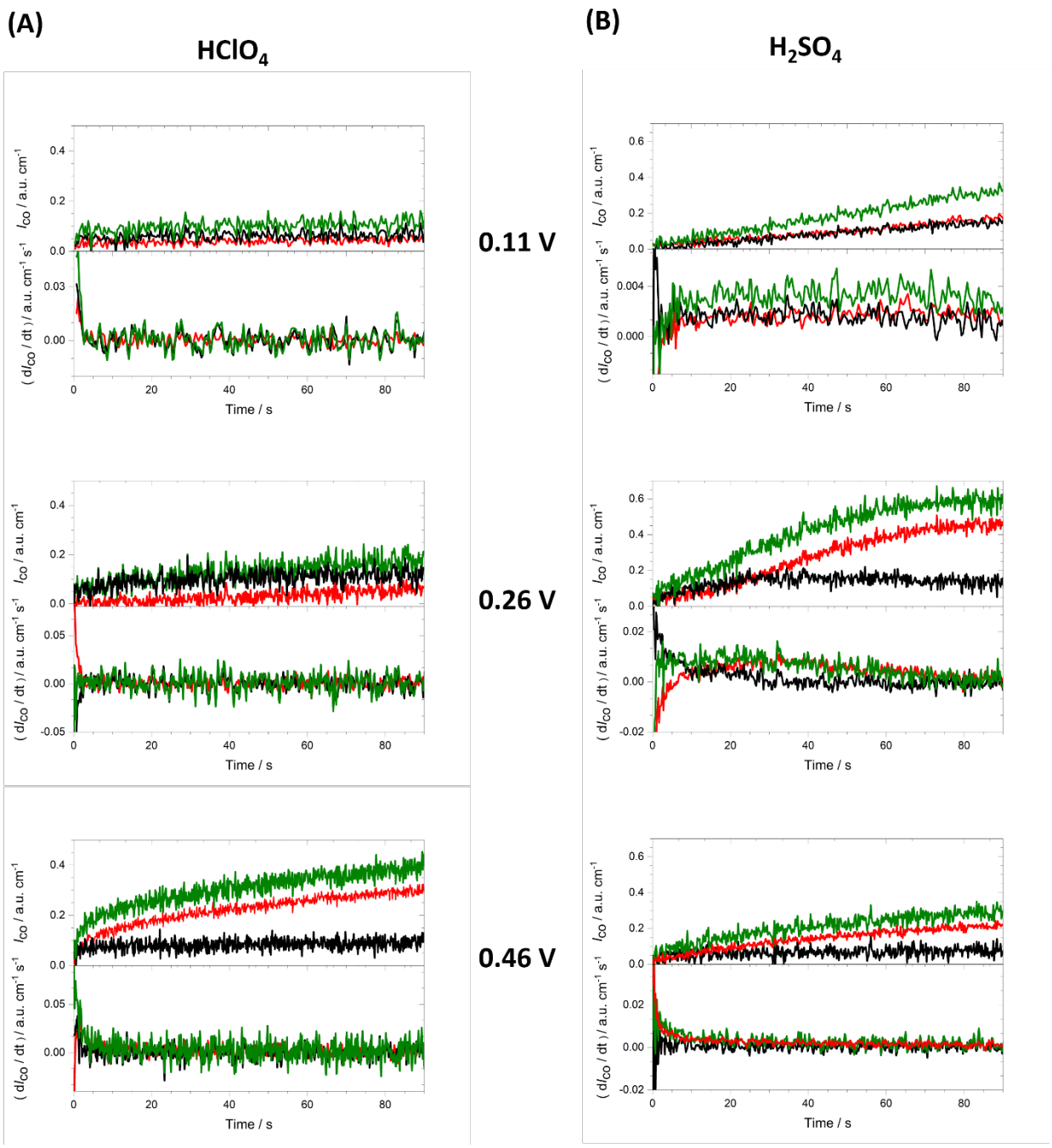

Figure S5. Time dependence of I_{CO_L} (red), $I_{CO_{B/CO_M}}$ (black) and $I_{CO_L} + I_{CO_{B/CO_M}}$ (green) (top panels) and of the derivatives of the corresponding raw, unsmoothed data with respect to time (lower panels) obtained from a series of time-resolved ATR-SEIRA spectra in 0.1 M $HClO_4$ **(A)** and 0.1 M H_2SO_4 **(B)** containing 0.01 M CH_3OH, recorded after a potential step from 0.96 and 0.91 V, respectively, to 0.11 (top), 0.26 (middle) and 0.46 (bottom) V. The derivatives were

smoothed using an adjacent average signal processing method with 70 **(A)** and 20 **(B)** points of window.

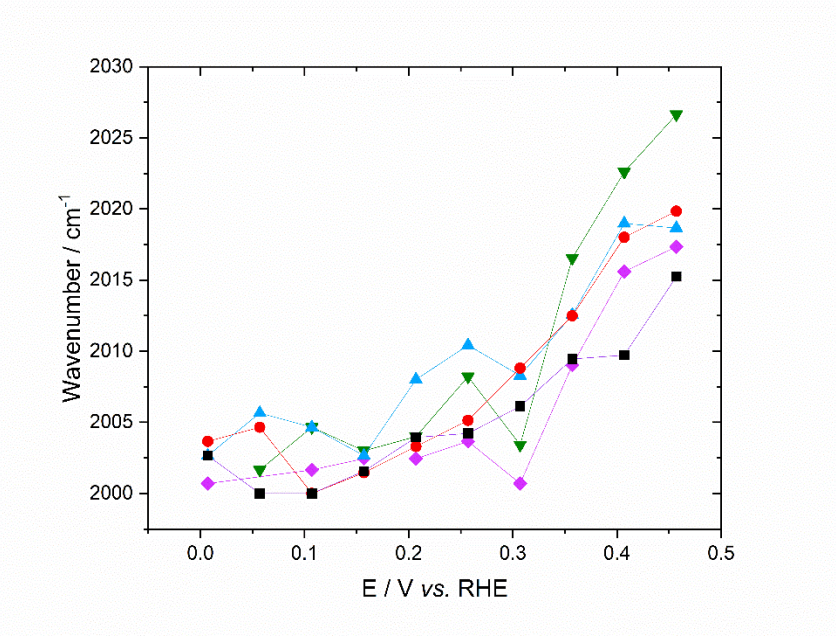

Figure. S6. Potential dependence of the C-O stretching frequency of linearly-bonded COad at the θ_CO→0 limit from a series of time-resolved ATR-SEIRA spectra after a potential step from 0.96 V in 0.1 M HClO4 containing CH3OH at the following concentrations : 0.01 M (purple rhombi), 0.02 M (inverted green triangles), 0.04 M (blue triangles), 0.065 M (red circles) and 0.1M (black square).